# CRISPR/Cas9 Mediated Gene Modification Ameliorates Abnormal Phenotypes in SCA3/MJD Disease Patient Derived Induced Pluripotent Stem Cells

**Lang He**
Xiangya Hospital Central South University
**Shang Wang**
Xiangya Hospital Central South University
**Huifang Zhao**
University of Science and Technology of China
**Shuai Li**
University of the Chinese Academy of Sciences
**Xiaobo Han**
University of the Chinese Academy of Sciences
**Zhao Chen**
Xiangya Hospital Central South University
**Chunrong Wang**
Xiangya Hospital Central South University
**Yun Peng**
Xiangya Hospital Central South University
**Huirong Peng**
Xiangya Hospital Central South University
**Linliu Peng**
Xiangya Hospital Central South University
**Yue Xie**
Xiangya Hospital Central South University
**Lijing Lei**
Xiangya Hospital Central South University
**Qi Deng**
Xiangya Hospital Central South University
**Linlin Wan**
Xiangya Hospital Central South University
**Na Wan**
Xiangya Hospital Central South University

**Hongyu Yuan**
Xiangya Hospital Central South University
**Yiqing Gong**
Xiangya Hospital Central South University
**Guangdong Zou**
Xiangya Hospital Central South University
**Zhiyuan Li**
Guangzhou Institutes of Biomedicine and Health
**Beisha Tang**
Xiangya Hospital Central South University
**Hong Jiang** (jianghong73868@126.com)
Department of Neurology, Xiangya Hospital, Central South University, Changsha, Hunan, China
https://orcid.org/0000-0003-2812-4120

---

**Research article**

**Keywords:** Spinocerebellar ataxia type 3/Machado-Joseph disease, CRISPR/Cas9, induced pluripotent stem cells, stem cell therapy, phenotypes

**Posted Date:** October 12th, 2020

**DOI:** https://doi.org/10.21203/rs.3.rs-88222/v1



---

# Abstract

**Background** Spinocerebellar ataxia type 3/Machado-Joseph disease (SCA3/MJD) is a progressive autosomal dominant neurodegenerative disease caused by abnormal CAG repeats in exon 10 of *ATXN3*. The accumulation of the mutant ataxin3 proteins carrying polyglutamine (polyQ) lead to selective degeneration of neurons. Therapeutic strategies were used to inhibit mutant *ATXN3* expression, including antisense oligonucleotides, RNA interference and more recently CRISPR/Cas9 genome-editing based approaches. Since the pathogenesis of SCA3 has not been fully elucidated, and no effective therapies can be used, it is crucial to investigate the pathogenesis and seek new therapeutic strategies of SCA3/MJD.

**Methods:** Here we used the paired sgRNA/Cas9 nickases and Cre-loxP mediated homologous recombination (HR) strategy to precisely modify the abnormal CAG expansions in the *ATXN3* of SCA3/MJD patient derived induced pluripotent stem cells (SCA3/MJD-iPSCs). Meanwhile, we investigated the disease related phenotypes in differentiated neurons, including electrophysiological characteristics, IC2-positive aggregations, mitochondrial membrane potentials (MMPs), glutathione (GSH) expressions, intracellular reactive oxygen species (ROS), $Ca^{2+}$ concentrations and malondialdehyde (MDA) levels.

**Results:** SCA3/MJD-iPSCs can be corrected by the replacement of the abnormal CAG expansions with normal repeats using HR. Besides, corrected SCA3/MJD-iPSCs retained pluripotent and normal karyotype, which could be differentiated into neuron cells (NCs) and maintained electrophysiological characteristics. The expression of differentiation markers and electrophysiological characteristics were similar among the control individuals, SCA3/MJD patients and isogenic control SCA3/MJD groups. Furthermore, this study proved that the phenotypic abnormalities in SCA3/MJD-iPSCs derived NCs, including aggregated polyQ toxic protein, decreased MMPs and GSH expressions, increased ROS, $Ca^{2+}$ concentrations and MDA levels, all were rescued in the corrected SCA3/MJD-NCs.

**Conclusion:** The present study firstly suggested that the genetically corrected SCA3/MJD-iPSCs and associated phenotypic abnormalities, which will provide an ideal models for molecular mechanism research and autologous stem cell therapy.


# Background

Spinocerebellar ataxia type 3/Machado-Joseph disease (SCA3/MJD) is the most common subtype of spinocerebellar ataxias (SCAs), accounting for about 60~70% of SCAs in Chinese population [1, 2].The pathogenesis of SCA3/MJD is due to the abnormal CAG repeats in the encoding region of *ATXN3*. The normal CAG repeats expand from 11 to 44, when the dynamic expansions up to 60~87, disease occurred [3-6]. CAG expansions in SCA3/MJD inversely correlates with age at onset (AAO), contributing to 50~80% of the AAO variation, suggesting that modifier genes, epigenetics and other environmental factors also affect the AAO. Besides, CAG expansion directly involves with disease progression [7-9]. Unstable CAG

expansions result in abnormal polyglutamine (polyQ) tract in ataxin-3 protein, forming neuronal intranuclear inclusions (NIIs) selectively accumulated in the cerebellum, brainstem, brain cortex, spinal cord, etc. Expanded polyQ protein affects various cellular activities via a gain of toxic functions, thus causing cell death [3]. Given that the pathogenesis of SCA3/MJD has not been elaborated completely, and no idea treatment methods have been achieved, it is urgent to study the pathogenic mechanism and explore new therapies of SCA3/MJD.

RNA interference (RNAi) inhibits gene expression by targeting the mRNA, which subsequently induce off-targeted sites (OTs) and degrade over time [10, 11]. Antisense oligonucleotide (ASO) deletes trinucleotide expansions, via non-selective-alleles (both wild type and mutant alleles) silencing *ATXN3 or HTT*, is another effective strategy to cure polyQ diseases [12-19]. Although the non-selective strategy can effectively improve the neuropathological changes and motor function in HD mice, the safety risk of its application in humans cannot be excluded [19]. However, specific targeting single nucleotide polymorphism (SNPs) in mutant allele to achieve permanent gene silencing, and without affecting the normal allele, is the ultimate targets of treatment [20, 21]. Therefore, it is of great significance to develop heritable gene therapies for permanently silencing DNA sequences. Clustered regularly interspaced short palindromic repeats (CRISPR/Cas9) mediated gene editing technique, has shown significant curative effects in treating polyQ cell and animal models [20-28].

Zinc finger nucleases and transcription activator like effector nucleases are the initial tools targeting DNA sequences permanently [29]. However, the latest genome-editing technology of small RNA-guided nuclease (sgRNA), which belongs to the CRISPR system, targets specific gene sites via the 20-nucleotide sgRNA targeting 5'-NGG of protospacer adjacent motif (PAM). Afterwards, the DNA upstream of PAM were cleaved by the Cas9 protein, and silencing targeted gene everlasting [30-32]. Hereafter, double-strand breaks (DSBs) could be repaired by non-homologous end joining (NHEJ) or homologous recombination (HR) mechanisms. NHEJ results in frameshift mutation in open reading frames, premature translation termination, and nonsense translation-mediated transcription degradation. However, HR can generate precisely defined modifications at target sites requiring external repair template, which compose traditional double-stranded DNA targeting structures with homologous arms on either side of the insertion sequences [32]. Moreover, combining Cas9 nickase (Cas9n) with paired sgRNAs to introduce directional DSBs can effectively cleave the target loci and reduce the occurrence of OTs [31]. Therefore, the combination of paired sgRNA/Cas9n and HR is effective tool aimed at precisely genome-editing in cell-based replacement therapy.

Human induced pluripotent stem cells (hiPSCs) carry the entire genetic background of patients and could be differentiated into unlimited source of interested cell populations. Increasingly, Cas9-directed genome-editing of iPSCs offers unprecedented opportunity for disease modeling, drug screening and cell replacement therapy for neurodegenerative diseases [3, 33, 34]. Previously, we obtained the urethral epithelial cells derived iPSCs from SCA3/MJD patients with 74/31 CAG repeats, which own the same mutant *ATXN3* as parental somatic cells, and capable of differentiating into neuronal cells (NCs), providing an ideal cell models for studying the pathological mechanisms and drug screening of

SCA3/MJD [35]. In this study, we use the paired sgRNA/Cas9n and HR strategy to precisely modify the abnormal CAG expansions in the *ATXN3* of SCA3/MJD-iPSCs. Meanwhile, we investigate the abnormal phenotypes such as mitochondrial dysfunction and oxidative stress activation in the corresponding broad-spectrum neurons, all were reversed in isogenic-corrected SCA3/MJD-NCs. Altogether, this study emphasis the use of isogenic control iPSCs from SCA3/MJD to investigate relevant molecular phenotypes in genetic backgrounds, and sets the crucial stage for the utility of these cells in cell replacement therapy.

# Methods

## Cloning of sgRNAs and donor DNA

Two guide sgRNAs (Additional file 8: Table S1) were designed to target the *ATXN3* using CRISPR design tool (E-CRISP□http://www.e-crisp.org/E-CRISP/) [36], and cloned into the spCas9 plasmids pX330-mcherry from Feng Zhang (Addgene #98750), adopted from Ran et al [32]. A 1.9 kb 5'homology arm and a 3.2 kb 3'homology arm containing 17 "CAG" repeats in the exon 10 of *ATXN3*, were cloned into the Hind□ and Not□ sites (Life Technologies, USA) of the pFlexible-DT HR targeting donor vector (loxP-pGK-puro-loxP).

## The activity of sgRNA/Cas9n in HEK293T cells

HEK293T cells were cultured in DMEM medium (High glucose, Gibco, USA) supplemented with 10% fetal bovine serum (FBS, Life Technologies, USA), $3\times10^5$ HEK293T cells were seeded 6 well plate and transfected with 3μg DNA using Effectene® Transfection Reagent (QIAGEN, Germany) according to the manufacturer's instructions. For testing the activity of sgRNA/Cas9n, after 48h transfection, the cells were lysed with NP40, targeted CAG repeats with P5~P6 primers by PCR amplification, and PCR products were purified, then digested with T7EN1 assay after denaturing and annealing reaction, and identified with 2% agarose gel. The percent of cutting rates were performed using ImageJ software.

## Nucleofection of sgRNA/Cas9n into iPSCs and positive clones screening

Amaxa nucleofection system (LONZA, Switzerland) of iPSCs was performed following the manufacturer's instructions. Briefly, hiPSCs were pre-treated with 10μM ROCK inhibitor Y-27632 (ROCKi, Selleck, USA) for 24h and dissociated into single cell suspension with accutase (Sigma, USA). $6\sim8\times10^5$ hiPSCs were plated in electroporated cuvette using solution□82ul supplemented with solution □18ul (Human stem cell Nucleofector Kit 2, LONZA, Switzerland). The cells were electro-transfected with 3μg sgRNA1 and sgRNA2, 5μg donor plasmids using program A-023 (LONZA, Switzerland). After electro-transfection, cells were immediately plated in mTeSR1 with ROCKi for 72h culture, and 0.3μg/ml puromycin was added to the medium. After 10~14 days selection, visible colonies were picked manually and transferred into 48 well plate, then the positive clones were screened using PCR primers (P1~P2 and P3~P4 primers)

performed with 2×Taq Plus Master Mix  (Vazyme, China). PCR products were run on a 2% gel-electrophoresis and further analyzed by capillary electrophoresis (*ATXN3*-FAM). In addition, the bands were purified and cloned into TA vectors and analyzed by Sanger sequencing of Beijing TsingKe Biotechnology Company, China.

## OTs analysis

We used GT-Scan website (https://gt-scan.csiro.au/gt-scan) [37] to detect potential OTs, potential sgRNAs OTs in human genome using the following criteria: NRG PAM, 3~4 mismatches. Primers were designed according to the potential 5 OTs of each sgRNA (Additional file 9: Table S2). The non-specific cutting of potential sgRNAs were verified by T7EN1 assay following the manufacturer's instructions (NEB).

## iPSCs culture and differentiation

iPSCs were reprogrammed from urines epithelial cells with the non-integration method (oriP/EBNA1-based episomal vector *pCEP4-O2SET2K* carrying the *OCT4* (*POU5F1*), *SOX2*, *SV40LT*, *KLF4* and *pCEP4-miR302–367* cluster as previously described [35, 38]. iPSCs were grown on Matrigel (Biocoat, China) coated plate, cultured daily with mTeSR1 medium (Stem Cell Technologies, Canada) and passaged with 0.5mM EDTA (Life technologies, USA) every 3~5 days.

According to the protocols for terminal cerebellar cortical differentiation [39], iPSCs were confluent to 90~100%, then the medium was switched to N2B27+2i differentiation medium [DMEM/F12 or Neurobasal medium (mixture rate: 1:1) with 1% N2, 2% B27, 1% non-essential amino acids (NEAA), 1% GlutaMax (all from Life Technologies, USA), 100μM β-mercaptoethanol (Sigma, USA), 2ug/ml heparin (Sigma, USA), 5ug/ml insulin (Sigma, USA), 1 μM Dorsomorphin (Sigma, USA) and 10 μM SB431542 (Selleck, China)], the medium was refreshed every day until 8 days culture, the neuroepithelial aggregates were picked into the Matrigel-coated 6 well plate for further differentiation in N2B27 medium without 2i, medium was changed daily. Around 14~18 days, the neural rosette structures appeared, the cells were suspension cultured in N2B27 medium for neural stem cells/neural precursor cells (NSCs/NPCs) expansion. After expansion 1~3 generations, the NSC aggregates enzymatically dissociated to single cells using accutase and cultured in N2B27 medium for final neuronal differentiation.

## Immunocytochemistry

Cells were fixed with 4% paraformaldehyde for 15 minutes at room temperature (RT). Then, the cells were permeabilized with 0.5% Triton X-100 (Sigma, USA) for 5 min and blocked with 10 % goat serum (Millipore, USA) diluted in 0.5% Triton X-100 and PBS for 30 minutes at RT. Primary antibodies were diluted into blocking liquid and incubated overnight at 4°C. Then, cells were transferred into secondary antibodies, and incubated for 1 hours at RT in dark. Nucleus was stained with DAPI (Beyotime, China) for 5 minutes. Coverslips were mounted with fluorescence quencher. Images were captured with IX73

Olympus inverted microscope (Olympus, Janpan) or confocal microscope imager LSM710 or LSM800 (Zeiss, Germany), and image analysis were performed with software ZEN (Zeiss, Germany). Neuronal marker of SYP1, PSD95, TUJ1, MAP2 and GABA were measured by the fluorescence quantitative analysis using ImageJ software. 5~8 images were analyzed from each images.

## Mitochondrial membrane potentials (MMPs) detection

The cell culture medium was removed, detached cells were collected and washed with PBS for 2~3 times. Then, the cells were added into JC-1 staining working solution and incubated for 30 min at 37℃. After incubation, the cells were washed 2 times with JC-1 staining buffer and performed with Flow cytometry (BD Accuri C6). Data was processed with Flow Jo software.

## ROS, intracellular $Ca^{2+}$, MDA and GSH measurement

The cell reactive oxygen species (ROS) were measured with DCFH-DA fluorescent probe, Fluo-4 AM for detecting $Ca^{2+}$, the Malondialdehyde (MDA) levels and glutathione (GSH) levels were detected by the Lipid Peroxidation Malondialdehyde Assay Kit and reduced glutathione/oxidized glutathione (GSH and GSSG Assay Kit) following the manufacturer's instructions (Beyotime, China), respectively. The detail procedures described in Supplementary Materials and Methods.

## Electrophysiology

Whole cell voltage clamp and current clamp techniques were used to conduct electrophysiological experiments at RT [40]. Neurons were grown on cover glass, which was placed in the center of cell perfusion tank. The cells were immersed in the artificially configured extracellular fluid, containing 95% $O_2$ and 5% $CO_2$. The resistance value of glass microelectrode used in the operation was about 8~10MΩ. Extracellular fluid consisted of artificially simulated cerebrospinal fluid, including NaCl 127mM, KCL 3mM, $MgSO_4$ 1mM, $NaHCO_3$ 26mM, $NaH2PO_4$ 1.25mM, $CaCl_2$ 2mM, and D-glutacose 10mM, PH 7.3~7.4. Intracellular solutions composed of potassium-methylsulfonate 140mM, NaCl 5mM, $CaCl_2$ 1mM, HEPES 10mM, EGTA 0.2mM, $ATPNa_2$ 3mM and $GTPNa_2$ 0.4mM, PH=7.2. In the current clamping mode, by recording and measuring the resting membrane potentials (RMPs) and spontaneous firing rate, the average value was 60s in the gap-free mode. Then, the RMPs of each cell was clamped to -70 mV as far as possible with steady currents. Action potentials (APs) threshold were recorded by depolarizing current steps (5pA, 20ms). Voltage-dependent ion channels recording: series resistance was compensated to about 90% before recording, the inward and outward currents were recorded. Action potential and current properties were analyzed using Clampfit 10.2 software. Postsynaptic potential recording: the spontaneous excitatory postsynaptic potentials (sEPSCs) were detected at -65mv clamping voltage. Moreover, the spontaneous inhibitory postsynaptic potentials (sIPSCs) were detected at 0mV clamping voltage, the data analyzed using Clampfit 10.2 and Origin8.6 software.

## Statistical analysis

The data were analyzed with GraphPad Prism 8.0. The double-tailed t test was used for two groups; multi-group data were analyzed using one-way ANOVA and Bonferroni post hoc test, all sample represent three or more independent experiments. The difference of $P<0.05$ was statistically significant.

# Results

## Analysis of paired *ATXN3*-sgRNA/Cas9n activity in HEK293T cells

Paired sgRNAs can enhance Cas9n-mediated DSBs to generate highly specific genome-editing, which could reduce OTs and enhance HR modification [31]. Considering for the distance and cleavage length of sgRNAs at the target gene, we designed a pair of sgRNAs (*ATXN*3_sgRNA1 and *ATXN3*_sgRNA2) for the upstream and downstream PAM regions of CAG repeat tract in exon 10 of *ATXN3* (Fig. 1a and

Additional file 8: Table S1). Cells were transfected with plasmids expressing both wtCas9 protein and sgRNA (Fig. 1b). SgRNAs targeting CAG repeats of *ATXN3* have been successfully constructed by Sanger sequencing (Fig. 1c). The first screening of sgRNA activity was performed in HEK293T cells. The transfection efficiency of HEK293T cells was 30~50% by immunofluorescence and flow cytometry after 24~48h transfection (Fig. 1d). The cellular genome was isolated after 48~72h transfection. PCR amplification of the CAG repeats in *ATXN3*, and subsequent T7EN1 assay resulted in multiple bands in both treated and untreated control cells, 630 amplified bands were produced in untreated cells. 116bp and 514bp bands appeared after sgRNA1 cleavage, while 253bp and 377bp bands were presented after sgRNA2 cleavage. The cleavage efficiency of sgRNA1 and sgRNA2 was 19.3% and 22.6% respectively (Fig. 1e). HEK293T cells contained 14 and 24 CAG duplicates in both alleles of *ATXN3* (Additional file 1: Figure S1). After treated with sgRNA1 and sgRNA2, the PCR amplification of targeting site and sequencing analysis showed bimodal and mixed signals (Fig. 1f). These results indicated that the designed sgRNAs have significant cleavage efficiency in vitro experiments.

## Gene correction of SCA3/MJD patient-derived iPSCs

To correct the disease mutation in SCA3/MJD-iPSCs and generate isogenic control lines, we adopt the CRISPR/Cas9 and Cre-loxP-mediated HR based genome-editing methods. We employed targeting donor construct (loxP-pGK-Puro-loxP), the donor cassette contains a 1919bp left arm and 3264bp right arm containing 17 CAG repeats based on the sgRNA1 cleavage site (intron 9), and successfully cloned into a pFlexible-DT vector (donor repair template), and puromycin-resistance gene (Puro) for positive clone screening (Fig. 2a). Firstly, we transfected 3ug paired sgRNAs/Cas9n (sgRNA1+sgRNA2) and 5ug donor repair template into the SCA3/MJD-iPSCs carrying 31/74 CAG expansions. The paired sgRNAs/Cas9n transfecting efficiency was 2.8% by flow cytometry (Fig. 2b). After post-electroporation for 72h, 300ng/ml Puro was added for selecting corrected clones. Targeted clones were selected for further culture in 13~18 days (Fig. 2c). Positive clones were identified by PCR using P1~P2 primers. The successfully corrected

cell lines contained 510bp and 3090bp, and identified 4 corrected lines (C3, C11, C12, C13), all did not detect any mutant bands (Fig. 2d). In addition, the positive clones were further verified by PCR (P3~P4 primers), and only two cell lines (C3, C12) contained 3787bp target bands (Additional file 2: Figure S2). We confirmed that paired sgRNAs effectively targeted CAG expansions in exon 10 of *ATXN3*.

Successful correction of the mutant *ATXN3* allele was verified by western blot using antibodies for ataxin3 protein (H9, MAB5360) (Fig. 2e). Of the 116 clones screened, 14 were targeted CAG expansions, of which 2 clones (C3 and C12) were confirmed by PCR screening (P1~P2 and P3~P4 primers) and western blot, accounting for about 1.7% of the screened positive clones. The HR rate is consistent with previously reported in HD-iPSCs [24] (Fig. 2f). Capillary electrophoresis and fragment length analysis showed that the corrected SCA3/MJD-iPSCs did not contain visible disease-causing *ATXN3* mutations (ie, CAG74). Meanwhile, the corrected SCA3/MJD-C3 and SCA3/MJD-C12 maintained 17/31 CAG repeats in *ATXN3* (Additional file 3: Figure S3).

Remarkably, ten potential OTs (Additional file 9: Table S2) for *ATXN3*-sgRNA/Cas9n were predicted by silico analysis using GT-Scan (http://gt-scan.braembl.org.au) [37]. The potential OTs of each sgRNAs were PCR-amplified and analyzed with T7EN1 assays. Our results showed no detectable OTs examined in the ten sites (Additional file 4: Figure S4).

## Corrected SCA3/MJD-iPSC remaining pluripotent characteristics

Previous study showed that parental SCA3/MJD-iPSCs retained disease-associated mutations and normal karyotype, expressing pluripotency markers, as well as have the potential to differentiate into three germ layers [35]. The pluripotent characteristics also kept in the genetically control SCA3/MJD-iPSCs (C3 and C12) (Fig. 3 and Additional file 5: Figure S5). Specifically, normal karyotype (Fig. 3d) and pluripotency markers of NANOG, SOX2, SSEA4 were measured by immunofluorescence staining (Fig. 3a) and flow cytometry (Fig. 3b). Endogenous expressing pluripotency markers of *NANOG*, *SOX2* and *OCT4* were evaluated by RT-qPCR (Fig. 3c). In vivo teratoma assay, the corrected clones showed the potential to differentiate into three germ layers, as shown by positive hematoxylin dyeing for glandular structure (endoderm), cartilage (mesoderm), and neural rosettes (ectoderm) (Fig. 3e).

## Differentiation of SCA3/MJD and isogenic control iPSCs into forebrain cortical neurons and hindbrain Purkinje progenitor cells

To generate mature neurons from SCA3/MJD-iPSCs, Koch et al. [41] differentiated iPSCs into long-term self-renewing neuroepithelium stem cells. The differentiation system has cortical neural and glial mixed populations after long-term proliferation. Given that studying iPSCs-derived forebrain neurons may shed light on the pathogenesis of SCA3/MJD, we used the monolayer culture method of cortical neurons, which experienced the stage of neural rosettes and mature neural differentiation [39]. Typical and mature neurons can be observed after about 60 days of neural induction (Fig. 4a). SCA3/MJD-iPSCs (74 CAG

repeats), corrected SCA3/MJD-iPSCs (C3 and C12, containing 17 and 31 CAG repeats, respectively) and control-iPSCs (Ctr1, 29 CAG repeats) were efficiently differentiated into forebrain NSCs after 16 days of neural induction. The NSCs markers of *PAX6*, *NESTIN*, *FOXG1*, *SOX1* and *OTX1D* were highly expressed on day 16 detected by RT-qPCR (Fig. 4b and Additional file 6: Figure S6). Moreover, PAX6 and NESTIN were positive staining by immunofluorescence (Figure 4c-f). At this stage, there was no significant difference in the NSCs markers expression among each group.

Using our protocols, 30~60 days after neuronal differentiation, all cells expressed mature NCs markers, including the majority of β-III-tubulin, MAP2 and GABA, as well as a small portion of glial fibrillary acidic protein (GFAP in astrocytes). The ratio of neurons to astrocytes (TUJ1/GFAP) was 2:1 (Fig. 5a and 5c). At this stage, there were no significant differences in TUJ1/GFAP and MAP2/GABA positive cells among the Ctrl-NCs, SCA3/MJD-NCs and corrected SCA3/MJD-NCs (C3, C12) groups (Fig. 5a-f).Therefore, our protocols of iPSCs differentiated into neurons and astrocytes was consistent with previous studies, in which the transformation of iPSCs led to a mixture of cultured neurons and astrocytes [41, 42]. Further analysis revealed that SYP1/PSD95, which is the pre- and post-synaptic marker of synaptic development, expressed similarly in four groups at days 40~60 differentiation as previously reported (Fig. 5g-h). Moreover, IC2 NIIs aggregates were only detected in SCA3/MJD-NCs compared with other groups (Fig. 5i).

Former studies have shown the susceptibility of hindbrain neurons in SCA3/MJD patients [3]. To conduct the cerebellar neurons, we adopted a specific developmental model of cerebellar tissue, by differentiating iPSCs into cerebellar Purkinje progenitor cells based on previous protocols (Additional file 7: Figure S7a) [43-46]. We detected the up-regulation of midbrain/hindbrain patterning markers, such as the *KIRRLE2*, *FGF8*, *WNT1*, *GBX2* and *OTX2*, by RT-qPCR on days 24 of differentiation (Additional file 7: Figure S7b). Immunofluorescence showed cerebellar precursor cells expressing KIRREL2/TUJ1 on days 24~32 (Additional file 7: Figure S7c). After 24~30 days of differentiation, the cerebellar progenitor cells in heterogeneous culture were sorted by KIRREL2$^+$, and the selected KIRREL2$^+$ Purkinje progenitor cells accounted for 19.2% by flow cytometry (Additional file 7: Figure S7d). However, the purified KIRREL2$^+$ cerebellar precursor cells need to be co-cultured with purified cerebellar granule cells, which came from newborn mice, for 2~3 months until the mature Purkinje cells (PCs) generation. We could not obtain enough vigorous cell populations after fluorescence-activated cell sorting. In the future, we are planning to obtain more vigorous cell populations by optimizing the Purkinje progenitor cells purification scheme, or selecting THY1$^+$ cell subpopulations for further exploring mature PCs differentiation strategies [46].

## Electrophysiological functions of SCA3/MJD-iPSCs differentiated cortical neurons

Next, we explored electrophysiological properties of the differentiated neurons. Whole-cell patch-clamp recording techniques were used to measure the intrinsic electrophysiological excitability of these differentiated cells for 6~7 weeks. Evoked action potentials (APs) displaying the excitable properties

under current clamp were recorded in SCA3/MJD-NCs (Fig. 6a). Robustly $Na^+$, $K^+$ and $Ca^{2+}$ inward and outward currents were detected in Ctr1-iPSCs, SCA3/MJD-iPSCs, and SCA3/MJD-C3-iPSCs derived NCs (Fig. 6b). Besides, the inward $Na^+$ and $Ca^{2+}$ currents can be blocked by TTX (1μM) and Cdcl2 (0.1mM) ion antagonist, respectively (Fig. 6c). Under the action of the depolarized current pulse, there was no significant difference in the inward or outward current peaks among the three groups (Fig. 6b). In order to assess the effect of *ATXN3* mutation on glutamatergic synaptic formation and excitatory synaptic transmission, both spontaneous glutamatergic sEPSCs and spontaneous GABAergic sIPSCs were recorded in whole-cell voltage-dependent recordings. Results showed that sEPSCs could be blocked by CNQX (AMPA receptor antagonist, 10μM), or MK801 (NMDA receptor antagonist, 10μM), respectively (Fig. 6d). Altogether, these data indicated that Glu mediated excitatory synaptic and GABA mediated inhibitory synaptic, input onto iPSC-derived cortical neurons, a study supported by previous studies [41]. The frequency and amplitude of sEPSCs were very similar in each group (Fig. 6e-f). In addition, the membrane capacitances, input resistances and RMPs also showed no significant difference among three groups (Fig. 6g-i). These findings suggested that TUJ1/MAP2-positive neurons exhibit electrophysiological properties, and there was no obvious difference across the three different iPSCs derived neurons.

## Reversal of mitochondrial dysfunction and oxidative stress activation in corrected SCA3/MJD- iPSCs derived NCs

Mitochondrial membrane potential is an effective method to evaluate mitochondrial function. In this study, mitochondrial membrane potential decreased significantly in SCA3/MJD-NCs compared with Ctr1-NCs, and corrected SCA3/MJD-NCs rescued the level of membrane potential decline (Fig. 7a-b). Studies showed that abnormal changes in intracellular ROS and $Ca^{2+}$ levels were correlated with various neurodegenerative diseases [47-50]. In the present study, the ROS and intracellular $Ca^{2+}$ levels were significantly higher in SCA3/MJD-NCs compared with Ctr1-NCs, while obviously decreased in the corrected SCA3/MJD-NCs (Fig. 7c-d). In addition, the expression of MDA increased, and GSH decreased in SCA3/MJD-NCs, but could be rescued in the corrected NCs (Fig. 7e-f). This findings indicated that the increased generation of oxygen free radicals, activated oxidative stress, and decreased antioxidant capacity in SCA3/MJD-NCs, were related to neuronal dysfunction [50, 51]. Moreover, ROS were activated in SCA3/MJD-NCs over time following $H_2O_2$ stimulation compared with Ctrl-NCs and isogenic control SCA3/MJD-NCs (Fig. 7g). Altogether, this study highlighted the likely contribution of mitochondrial dysfunction and oxidative stress activation to the pathogenesis of SCA3/MJD.

## Discussion

Multiple therapies have been described for SCA3/MJD related polyQ diseases in recent years. Studies reported that knockdown of both m*ATXN3* and wt*ATXN3* alleles using RNAi and ASO, were a double-edged sword to SCA3/MJD models. Therefore, strategies aimed at selective silencing mutant alleles are developing rapidly [10, 15, 18, 19, 52]. In this study, we delivered paired sgRNA/Cas9n and donor DNA as modification templates to achieve HR repair, which was consistent with previous HD studies [24, 25, 53].

The efficiency of paired Cas9n genome-editing depends on the activity of paired sgRNA/Cas9n and the length of target sequences [31, 54]. SgRNA1 and sgRNA2 displayed cleavage activity in HEK293T cells, and the efficiency reached up to 19.3% and 22.6%, respectively. The present study demonstrated that paired sgRNA/Cas9n and HR strategies could modify the CAG repeats in exon 10 of *ATXN3*, then silencing the mutant ataxin3 protein effectively and specifically. Finally, isogenic control SCA3/MJD-iPSCs containing 17/31 CAG repeats were produced, and the targeted efficiency was 1.7%. Moreover, the safety of paired sgRNA/Cas9n strategy were confirmed by T7EN1 assay, and no potential OTs were detected.

This strategy provided a valuable model for further investigating molecular mechanisms of SCA3/MJD. In previous studies, deleting the CAG expansions was the main method to silence m*ATXN3* [13, 18, 26, 27]. More recently, the CRISPR/Cas9 system has been used to permanently clear the CAG expansions in exon 10 of *ATXN3* using paired sgRNAs/Cas9n. The stop codon appeared in exon 11, forming truncated ataxin3 protein, which still retained its ubiquitinating function [27]. Additionally, Xu et al showed that corrected HD-hiPSCs were established with seamless excision of the selection cassette, by targeting the exon 1-intron junction region in *HTT* with paired sgRNAs/Cas9n and piggyBac transposon-based approaches [25]. Although the drug screening gene was not removed in the present study, insertion of Puro selection cassettes in targeted intron region may not affect *ATXN3* expression. However, traditional Cre-loxP-mediated HR system was a specific gene manipulation tool, and it was inefficient [55]. Besides, Shin et al designed specific SNPs targeted PAM sites for the *mHTT* alleles, in order to specifically silencing the *mHTT* without affecting the *wtHTT* [20, 21]. Therefore, site-specific genome-editing technology improves editing efficiency effectively, providing a better strategy for treating SCA3/MJD related polyQ diseases.

Isogenic control SCA3/MJD-iPSCs (C3 and C12) maintained the pluripotency characteristics, which laying a valuable foundation for subsequent cellular phenotypic studies. Gene-corrected SCA3/MJD-iPSCs can be differentiated into cortical neurons and Purkinje precursor cells, referring to the previous protocols [39, 41, 43-45, 56, 57]. NSCs markers NESTIN and PAX6, as well as Purkinje precursor cells marker KIRREL2$^{+}$, showed no significant difference among the Ctrl-NSCs, SCA3/MJD-NSCs and corrected SCA3/MJD-NSCs groups. The results indicated m*ATXN3* did not affect the differentiation process of neurons in early stage. Furthermore, the expression of neuron markers (TUJ1/GFAP and MAP2/GABA)) and presynaptic and postsynaptic markers (SYP1/PSD95) also displayed no obviously difference in the four groups. Altogether, our study demonstrated that there are no discernable differences in the neuronal differentiation systems.

The present study also found IC2 positive polyQ proteins in SCA3/MJD-NCs, and the isogenic control SCA3/MJD-iPSCs reversed this phenotypic change. Studies suggested that polyQ chains had toxic effects, mainly gathered in the nucleus and cytoplasm of neurons, especially in the deep cerebellar nuclei, leading to selective neurotoxicity, progressive neuronal degeneration and morphological changes [3, 17]. In addition, previous studies showed that no toxic aggregates formed in the polyQ diseases cell models, under the absence of external stress or proteasome stimulation culture conditions, and non-pathological

ataxin3 distributed throughout nucleus and cytoplasm, while nuclear translocation occurred rapidly after the proteotoxic induction [58-60]. However, Moore indicated that ataxin3 expressed diffusely throughout cytoplasm and nucleus in WT-NSCs and WT-NCs, wherever, rubust *ATXN3* cytoplasmic aggregates formed in large, round, juxtanuclear and occasional round *ATXN3*-positive inclusions in SCA3/MJD-NSCs and SCA3/MJD-NCs; Moreover, no more NIIs produced in the differentiated SCA3/MJD-NSCs and SCA3/MJD-NCs, compared with the undifferentiated SCA3/MJD-ESCs [58]. Besides, Chuang et al. differentiated the SCA2-iPSCs and SCA3/MJD-iPSCs into highly expressed TUJ1/MAP2$^{+}$ cerebral cortical neurons, which detected IC2 aggregations in NCs, while not finding in Ctr1-NCs [61]. The afore-mentioned results confirmed the aggregates formation in m*ATXN3* cell models under normal stress-free culture conditions, which related to neurotoxicity. We further examined whether the differentiated neurons displayed electrophysiological function, which is the basic characteristic of neurons. It was found that SCA3/MJD-NCs could generate APs, $Na^{+}$, $K^{+}$ and $Ca^{2+}$ currents and postsynaptic currents. Indeed, no discernable differences observed, regarding to electrophysiological parameters in all sample groups. It reflects the heterogeneity of neuron types resulting from the adopted differentiation protocol to a large extent, rather than the differences caused by genotypic mutations.

Studies found that increased intracellular oxidative stresses, such as increased ROS concentration, $Ca^{2+}$ influx, MDA level, and decreased GSH, can lead to DNA, lipid and protein damages, thus causing peroxidation, activated oxidative stress and cell death. [47, 50, 51, 53, 62]. In this study, we displayed activated mitochondrial ROS, increased $Ca^{2+}$ internal flow, and MDA content, and decreased MMPs and GSH antioxidant levels in SCA3/MJD-NCs, compared with Ctrl-NCs, and corrected SCA3/MJD-NCs. However, the latter reversed the phenotypic abnormalities. The outcomes indicated that mitochondria and oxidative stress dysfunction were the important physiological mechanisms triggering neuronal injury in SCA3/MJD. Previous studies also indicated that mutant ataxin3 produced truncated C-terminal fragments in SCA3/MJD models after proteolysis, leading to increased mitochondrial division, decreased MMPs, increased ROS level and cell death [51, 63]. Moreover, increased glutamate levels in synaptic cleft can activate receptors on neighboring neurons, contributing to the excessive and continuous increase of free $Ca^{2+}$ in neurons, thus promoting the vicious cycle of neuronal injury [48]. The phenotypic abnormalities occurred in SCA3/MJD stem cell models were different from previous studies, which lay a valuable cellular models for pathological mechanism research. Altogether, these results may indicate that mutant ataxin3 could enhance $Ca^{2+}$ release from endoplasmic reticulum storages, then causing $Ca^{2+}$ overload and eventually cell death, accompanied by mitochondrial permeability, oxidative stress, cytoskeletal tissue destruction, and/or calpain activation [47-50].

However, this study also has some limitations. Firstly, genome-wide expression analysis should be performed on SCA3/MJD and genetically controlled cell lines, to determine whether there are any variations in OTs and SNPs variants. Global differential gene expression analysis is also needed, to identify transcriptional changes in SCA3/MJD and isogenic control lines [25]. Secondly, the main neuropathologic features of SCA3/MJD is the preferential loss of neurons in deep cerebellar nucleus and brainstem, while iPSCs differentiated cerebral cortical neurons cannot fully represent the neuropathologic

alterations of SCA3/MJD. Indeed, the decrease of PCs discharge frequency in SCAs mouse model was related to the abnormality of $K^+$ channel [15, 16]. It is necessary to differentiate into PCs and monitor the electrophysiological changes to investigate whether there are any differences among groups. Thirdly, mutant ataxin3 may affect mitochondrial respiratory and energy metabolism, which are related to mitochondrial dysfunction caused by biological energy deficiency [51, 64]. However, the bioenergy measurement has not been carried out in present study, and its relationship between bioenergy and respiratory function should be further explored.

## Conclusions

In summary, the present study firstly confirmed that paired sgRNA/Cas9n and Cre-loxP mediated HR strategy can realize precisely modification in SCA3/MJD-iPSCs, and no mutant ataxin3 protein were detected in genetically modified SCA3/MJD-iPSCs. Moreover, isogenic control SCA3/MJD-iPSCs retained pluripotent and normal karyotypes, which could be differentiated into NCs and maintained its electrophysiological characteristics. Besides, phenotypic abnormalities were identified in SCA3/MJD-NCs, including deficits in mitochondrial function and activated oxidative stress, all were rescued in corrected SCA3/MJD-iPSCs. Thus, the utility of paired sgRNA/Cas9n and HR approach provides a powerful and attractive stem cell therapy for SCA3/MJD related polyQ diseases.

## List Of Abbreviations

SCA3/MJD: Spinocerebellar ataxia type 3/Machado-Joseph disease; polyQ: polyglutamine; iPSCs: induced pluripotent stem cells; HR: homologous recombination; SCAs: spinocerebellar ataxias; AAO: age at onset; RNAi: RNA interference; OTs: off-targeted sites; SNPs: single nucleotide polymorphism; ASO: Antisense oligonucleotide; CRISPR/Cas9: Clustered regularly interspaced short palindromic repeats; sgRNA: small RNA-guided nuclease; NIIs: neuronal intranuclear inclusions; DSBs: double-strand breaks; NHEJ: non-homologous end joining; Cas9n: Cas9 nickase; NSCs/NPCs: neural stem cells/neural precursor cells; RT: room temperature; MMPs: mitochondrial membrane potentials; RMPs: resting membrane potentials; APs: Action potentials; sEPSCs: spontaneous excitatory postsynaptic potentials; sIPSCs: spontaneous inhibitory postsynaptic potentials; NCs: neuronal cells; Ctr1-iPSCs: Control-iPSCs; PCs: Purkinje cells; ROS: reactive oxygen species; GSH: glutathione; MDA: Malondialdehyde.

## Declarations

# Acknowledgements

We would like to thank JQT, XHL, QL, and YCP for critical reading and revising of this manuscript. The authors would like to thank Guangzhou Institutes of Biomedicine and Health for the experiment perform.

# Authors' contributions

HJ and LH conceived and designed the experiments. LH performed the experiments with the support from HFZ, SL and XBH. ZC, CRW, YP, HRP, LLP, YX, LJL, QD, LLW, NW, HYY, YQG and GDZ analyzed the data. LH wrote the manuscript, SW revised the manuscript. ZYL, BST and HJ reviewed and supervised the manuscript. All authors read and approved the final manuscript.

# Funding

This study was funded by the National Key Research and Development Program of China (No. 2016YFC0905100 and No.2016YFC0901504 to H Jiang; No. 2016YFC1306000 to B Tang), the National Natural Science Foundation of China (No. 81771231 and No. 81974176 to H Jiang; No. 81901169 to Z Chen; No.81901305 to C Wang; No. 81600995 to Y Shi), the Innovation Research Group Project of Natural Science Foundation of Hunan Province (No.2020JJ1008 to H Jiang), the Scientific Research Foundation of Health Commission of Hunan Province (No. B2019183 to H Jiang), the Key Research and Development Program of Hunan Province (No. 2018SK2092 to H Jiang), the Innovative Research and Development Program of Development and Reform Commission of Hunan Province to H Jiang, the Natural Science Foundation of Hunan Province (No.2019JJ40363 to R Qiu), the Clinical an ehabilitation Funds of Peking University Weiming Biotech Group (No. xywm2015l10 to H Jiang), and the Youth Foundation of Xiangya Hospital (No. 2017Q03 to Z Chen, No. 2018Q05 to C Wang). Guangzhou Regenerative Medicine and Health Guangdong

Laboratory (No. 2018GZR110105020 to Z Li). The National Natural Science Foundation of China (No. 31671211 to Z Li). Science and Technology Planning Project of Guangdong Province, China (No. 2017B030314056 to Z Li).

# Availability of data and materials

The datasets used and analyzed during the current study are available from the corresponding author on reasonable request.

# Ethics approval and consent to participate

All experiments were performed according to human stem cell and animal use protocols that were approved by the medical research ethics committee of Xiangya Hospital of Central South University (No.201412458).

# Consent for publication

Not applicable

# Competing interests

The authors declare that they have no competing interests.

# Authors' information

Not applicable

# References


1. Z. Chen, P. Wang, C. Wang, Y. Peng, X. Hou, X. Zhou, et al. Updated frequency analysis of spinocerebellar ataxia in China. Brain. 2018;141: p. e22.
2. R.P. Maas, J. van Gaalen, T. Klockgether, and B.P. van de Warrenburg The preclinical stage of spinocerebellar ataxias. Neurology. 2015;85: p. 96-103.
3. S. Naphade, K.T. Tshilenge, and L.M. Ellerby Modeling Polyglutamine Expansion Diseases with Induced Pluripotent Stem Cells. Neurotherapeutics. 2019;16: p. 979-998.
4. C. Costa Mdo and H.L. Paulson Toward understanding Machado-Joseph disease. Prog Neurobiol. 2012;97: p. 239-57.
5. T. Ashizawa, G. Öz, and H.L. Paulson Spinocerebellar ataxias: prospects and challenges for therapy development. Nat Rev Neurol. 2018;14: p. 590-605.
6. H.L. Paulson, V.G. Shakkottai, H.B. Clark, and H.T. Orr Polyglutamine spinocerebellar ataxias - from genes to potential treatments. Nat Rev Neurosci. 2017;18: p. 613-626.
7. Z. Chen, J. Sequeiros, B. Tang, and H. Jiang Genetic modifiers of age-at-onset in polyglutamine diseases. Ageing Res Rev. 2018;48: p. 99-108.
8. Z. Chen, C. Zheng, Z. Long, L. Cao, X. Li, H. Shang, et al. (CAG)n loci as genetic modifiers of age-at-onset in patients with Machado-Joseph disease from mainland China. Brain. 2016;139: p. e41.
9. C. Wang, H. Peng, J. Li, D. Ding, Z. Chen, Z. Long, et al. Alteration of methylation status in the ATXN3 gene promoter region is linked to the SCA3/MJD. Neurobiol Aging. 2017;53: p. 192.e5-192.e10.
10. C. Costa Mdo, K. Luna-Cancalon, S. Fischer, N.S. Ashraf, M. Ouyang, R.M. Dharia, et al. Toward RNAi therapy for the polyglutamine disease Machado-Joseph disease. Mol Ther. 2013;21: p. 1898-908.
11. A. Kotowska-Zimmer, Y. Ostrovska, and M. Olejniczak Universal RNAi Triggers for the Specific Inhibition of Mutant Huntingtin, Atrophin-1, Ataxin-3, and Ataxin-7 Expression. Mol Ther Nucleic Acids. 2020;19: p. 562-571.
12. L.R. Moore, G. Rajpal, I.T. Dillingham, M. Qutob, K.G. Blumenstein, D. Gattis, et al. Evaluation of Antisense Oligonucleotides Targeting ATXN3 in SCA3 Mouse Models. Mol Ther Nucleic Acids. 2017;7: p. 200-210.
13. M.M. Evers, H.D. Tran, I. Zalachoras, B.A. Pepers, O.C. Meijer, J.T. den Dunnen, et al. Ataxin-3 protein modification as a treatment strategy for spinocerebellar ataxia type 3: removal of the CAG containing

exon. Neurobiol Dis. 2013;58: p. 49-56.

14. L.J.A. Toonen, F. Rigo, H. van Attikum, and W.M.C. van Roon-Mom Antisense Oligonucleotide-Mediated Removal of the Polyglutamine Repeat in Spinocerebellar Ataxia Type 3 Mice. Mol Ther Nucleic Acids. 2017;8: p. 232-242.
15. H.S. McLoughlin, L.R. Moore, R. Chopra, R. Komlo, M. McKenzie, K.G. Blumenstein, et al. Oligonucleotide therapy mitigates disease in spinocerebellar ataxia type 3 mice. Ann Neurol. 2018;84: p. 64-77.
16. D.R. Scoles, P. Meera, M.D. Schneider, S. Paul, W. Dansithong, K.P. Figueroa, et al. Antisense oligonucleotide therapy for spinocerebellar ataxia type 2. Nature. 2017;544: p. 362-366.
17. H.S. McLoughlin, L.R. Moore, and H.L. Paulson Pathogenesis of SCA3 and implications for other polyglutamine diseases. Neurobiol Dis. 2020;134: p. 104635.
18. A.C. Silva, D.D. Lobo, I.M. Martins, S.M. Lopes, C. Henriques, S.P. Duarte, et al. Antisense oligonucleotide therapeutics in neurodegenerative diseases: the case of polyglutamine disorders. Brain. 2020;143: p. 407-429.
19. S. Esteves, S. Duarte-Silva, and P. Maciel Discovery of Therapeutic Approaches for Polyglutamine Diseases: A Summary of Recent Efforts. Med Res Rev. 2017;37: p. 860-906.
20. J.W. Shin, K.H. Kim, M.J. Chao, R.S. Atwal, T. Gillis, M.E. MacDonald, et al. Permanent inactivation of Huntington's disease mutation by personalized allele-specific CRISPR/Cas9. Hum Mol Genet. 2016;25: p. 4566-4576.
21. A.M. Monteys, S.A. Ebanks, M.S. Keiser, and B.L. Davidson CRISPR/Cas9 Editing of the Mutant Huntingtin Allele In Vitro and In Vivo. Mol Ther. 2017;25: p. 12-23.
22. N. Kolli, M. Lu, P. Maiti, J. Rossignol, and G.L. Dunbar CRISPR-Cas9 Mediated Gene-Silencing of the Mutant Huntingtin Gene in an In Vitro Model of Huntington's Disease. Int J Mol Sci. 2017;18: p.
23. S. Yang, R. Chang, H. Yang, T. Zhao, Y. Hong, H.E. Kong, et al. CRISPR/Cas9-mediated gene editing ameliorates neurotoxicity in mouse model of Huntington's disease. J Clin Invest. 2017;127: p. 2719-2724.
24. M.C. An, N. Zhang, G. Scott, D. Montoro, T. Wittkop, S. Mooney, et al. Genetic correction of Huntington's disease phenotypes in induced pluripotent stem cells. Cell Stem Cell. 2012;11: p. 253-63.
25. X. Xu, Y. Tay, B. Sim, S.I. Yoon, Y. Huang, J. Ooi, et al. Reversal of Phenotypic Abnormalities by CRISPR/Cas9-Mediated Gene Correction in Huntington Disease Patient-Derived Induced Pluripotent Stem Cells. Stem Cell Reports. 2017;8: p. 619-633.
26. M. Dabrowska, W. Juzwa, W.J. Krzyzosiak, and M. Olejniczak Precise Excision of the CAG Tract from the Huntingtin Gene by Cas9 Nickases. Front Neurosci. 2018;12: p. 75.
27. S. Ouyang, Y. Xie, Z. Xiong, Y. Yang, Y. Xian, Z. Ou, et al. CRISPR/Cas9-Targeted Deletion of Polyglutamine in Spinocerebellar Ataxia Type 3-Derived Induced Pluripotent Stem Cells. Stem Cells Dev. 2018;27: p. 756-770.

28. F.K. Ekman, D.S. Ojala, M.M. Adil, P.A. Lopez, D.V. Schaffer, and T. Gaj CRISPR-Cas9-Mediated Genome Editing Increases Lifespan and Improves Motor Deficits in a Huntington's Disease Mouse Model. Mol Ther Nucleic Acids. 2019;17: p. 829-839.
29. G.F. Richard Shortening trinucleotide repeats using highly specific endonucleases: a possible approach to gene therapy? Trends Genet. 2015;31: p. 177-86.
30. J.A. Doudna and E. Charpentier Genome editing. The new frontier of genome engineering with CRISPR-Cas9. Science. 2014;346: p. 1258096.
31. F.A. Ran, P.D. Hsu, C.Y. Lin, J.S. Gootenberg, S. Konermann, A.E. Trevino, et al. Double nicking by RNA-guided CRISPR Cas9 for enhanced genome editing specificity. Cell. 2013;154: p. 1380-9.
32. F.A. Ran, P.D. Hsu, J. Wright, V. Agarwala, D.A. Scott, and F. Zhang Genome engineering using the CRISPR-Cas9 system. Nat Protoc. 2013;8: p. 2281-2308.
33. K. Takahashi, K. Tanabe, M. Ohnuki, M. Narita, T. Ichisaka, K. Tomoda, et al. Induction of pluripotent stem cells from adult human fibroblasts by defined factors. Cell. 2007;131: p. 861-72.
34. D.A. Robinton and G.Q. Daley The promise of induced pluripotent stem cells in research and therapy. Nature. 2012;481: p. 295-305.
35. L. He, W. Ye, Z. Chen, C. Wang, H. Zhao, S. Li, et al. Generation of an induced pluripotent stem cell line (XHCSUi001-A) from urine cells of a patient with spinocerebellar ataxia type 3. Stem Cell Res. 2019;40: p. 101555.
36. F. Heigwer, G. Kerr, and M. Boutros E-CRISP: fast CRISPR target site identification. Nat Methods. 2014;11: p. 122-3.
37. A. O'Brien and T.L. Bailey GT-Scan: identifying unique genomic targets. Bioinformatics. 2014;30: p. 2673-5.
38. L. He, H. Zhao, S. Li, X. Han, Z. Chen, C. Wang, et al. Generation of induced pluripotent stem cell line (CSUXHi002-A) from a patient with spinocerebellar ataxia type 1. Stem Cell Res. 2020;45: p. 101816.
39. Y. Shi, P. Kirwan, and F.J. Livesey Directed differentiation of human pluripotent stem cells to cerebral cortex neurons and neural networks. Nat Protoc. 2012;7: p. 1836-46.
40. J. Liu, C. Gao, W. Chen, W. Ma, X. Li, Y. Shi, et al. CRISPR/Cas9 facilitates investigation of neural circuit disease using human iPSCs: mechanism of epilepsy caused by an SCN1A loss-of-function mutation. Transl Psychiatry. 2016;6: p. e703.
41. P. Koch, P. Breuer, M. Peitz, J. Jungverdorben, J. Kesavan, D. Poppe, et al. Excitation-induced ataxin-3 aggregation in neurons from patients with Machado-Joseph disease. Nature. 2011;480: p. 543-6.
42. J. Hamilton, T. Brustovetsky, A. Sridhar, Y. Pan, T.R. Cummins, J.S. Meyer, et al. Energy Metabolism and Mitochondrial Superoxide Anion Production in Pre-symptomatic Striatal Neurons Derived from Human-Induced Pluripotent Stem Cells Expressing Mutant Huntingtin. Mol Neurobiol. 2020;57: p. 668-684.
43. K. Muguruma, A. Nishiyama, Y. Ono, H. Miyawaki, E. Mizuhara, S. Hori, et al. Ontogeny-recapitulating generation and tissue integration of ES cell-derived Purkinje cells. Nat Neurosci. 2010;13: p. 1171-80.

44. K. Muguruma, A. Nishiyama, H. Kawakami, K. Hashimoto, and Y. Sasai Self-organization of polarized cerebellar tissue in 3D culture of human pluripotent stem cells. Cell Rep. 2015;10: p. 537-50.
45. S. Wang, B. Wang, N. Pan, L. Fu, C. Wang, G. Song, et al. Differentiation of human induced pluripotent stem cells to mature functional Purkinje neurons. Sci Rep. 2015;5: p. 9232.
46. M. Sundberg, I. Tochitsky, D.E. Buchholz, K. Winden, V. Kujala, K. Kapur, et al. Purkinje cells derived from TSC patients display hypoexcitability and synaptic deficits associated with reduced FMRP levels and reversed by rapamycin. Mol Psychiatry. 2018;23: p. 2167-2183.
47. A. Singh, R. Kukreti, L. Saso, and S. Kukreti Oxidative Stress: A Key Modulator in Neurodegenerative Diseases. Molecules. 2019;24: p.
48. C. Angeloni, M. Gatti, C. Prata, S. Hrelia, and T. Maraldi Role of Mesenchymal Stem Cells in Counteracting Oxidative Stress-Related Neurodegeneration. Int J Mol Sci. 2020;21: p.
49. X. Chen, T.S. Tang, H. Tu, O. Nelson, M. Pook, R. Hammer, et al. Deranged calcium signaling and neurodegeneration in spinocerebellar ataxia type 3. J Neurosci. 2008;28: p. 12713-24.
50. J.D. Da Silva, A. Teixeira-Castro, and P. Maciel From Pathogenesis to Novel Therapeutics for Spinocerebellar Ataxia Type 3: Evading Potholes on the Way to Translation. Neurotherapeutics. 2019;16: p. 1009-1031.
51. Y.C. Yu, C.L. Kuo, W.L. Cheng, C.S. Liu, and M. Hsieh Decreased antioxidant enzyme activity and increased mitochondrial DNA damage in cellular models of Machado-Joseph disease. J Neurosci Res. 2009;87: p. 1884-91.
52. R.A.M. Buijsen, L.J.A. Toonen, S.L. Gardiner, and W.M.C. van Roon-Mom Genetics, Mechanisms, and Therapeutic Progress in Polyglutamine Spinocerebellar Ataxias. Neurotherapeutics. 2019;16: p. 263-286.
53. J. Ooi, S.R. Langley, X. Xu, K.H. Utami, B. Sim, Y. Huang, et al. Unbiased Profiling of Isogenic Huntington Disease hPSC-Derived CNS and Peripheral Cells Reveals Strong Cell-Type Specificity of CAG Length Effects. Cell Rep. 2019;26: p. 2494-2508.e7.
54. P. Mali, J. Aach, P.B. Stranges, K.M. Esvelt, M. Moosburner, S. Kosuri, et al. CAS9 transcriptional activators for target specificity screening and paired nickases for cooperative genome engineering. Nat Biotechnol. 2013;31: p. 833-8.
55. F. Yang, C. Liu, D. Chen, M. Tu, H. Xie, H. Sun, et al. CRISPR/Cas9-loxP-Mediated Gene Editing as a Novel Site-Specific Genetic Manipulation Tool. Mol Ther Nucleic Acids. 2017;7: p. 378-386.
56. L.M. Watson, M.M.K. Wong, J. Vowles, S.A. Cowley, and E.B.E. Becker A Simplified Method for Generating Purkinje Cells from Human-Induced Pluripotent Stem Cells. Cerebellum. 2018;17: p. 419-427.
57. Y. Ishida, H. Kawakami, H. Kitajima, A. Nishiyama, Y. Sasai, H. Inoue, et al. Vulnerability of Purkinje Cells Generated from Spinocerebellar Ataxia Type 6 Patient-Derived iPSCs. Cell Rep. 2016;17: p. 1482-1490.
58. L.R. Moore, L. Keller, D.D. Bushart, R.G. Delatorre, D. Li, H.S. McLoughlin, et al. Antisense oligonucleotide therapy rescues aggresome formation in a novel spinocerebellar ataxia type 3

human embryonic stem cell line. Stem Cell Res. 2019;39: p. 101504.

59. C.P. Reina, X. Zhong, and R.N. Pittman Proteotoxic stress increases nuclear localization of ataxin-3. Hum Mol Genet. 2010;19: p. 235-49.
60. S. Koyuncu, I. Saez, H.J. Lee, R. Gutierrez-Garcia, W. Pokrzywa, A. Fatima, et al. The ubiquitin ligase UBR5 suppresses proteostasis collapse in pluripotent stem cells from Huntington's disease patients. Nat Commun. 2018;9: p. 2886.
61. C.Y. Chuang, C.C. Yang, B.W. Soong, C.Y. Yu, S.H. Chen, H.P. Huang, et al. Modeling spinocerebellar ataxias 2 and 3 with iPSCs reveals a role for glutamate in disease pathology. Sci Rep. 2019;9: p. 1166.
62. Y. Wang, M. Zhang, Z. Li, J. Yue, M. Xu, Y. Zhang, et al. Fine particulate matter induces mitochondrial dysfunction and oxidative stress in human SH-SY5Y cells. Chemosphere. 2019;218: p. 577-588.
63. J.Y. Hsu, Y.L. Jhang, P.H. Cheng, Y.F. Chang, S.H. Mao, H.I. Yang, et al. The Truncated C-terminal Fragment of Mutant ATXN3 Disrupts Mitochondria Dynamics in Spinocerebellar Ataxia Type 3 Models. Front Mol Neurosci. 2017;10: p. 196.
64. K. Wiatr, P. Piasecki, Ł. Marczak, P. Wojciechowski, M. Kurkowiak, R. Płoski, et al. Altered Levels of Proteins and Phosphoproteins, in the Absence of Early Causative Transcriptional Changes, Shape the Molecular Pathogenesis in the Brain of Young Presymptomatic Ki91 SCA3/MJD Mouse. Mol Neurobiol. 2019;56: p. 8168-8202.

# Figures

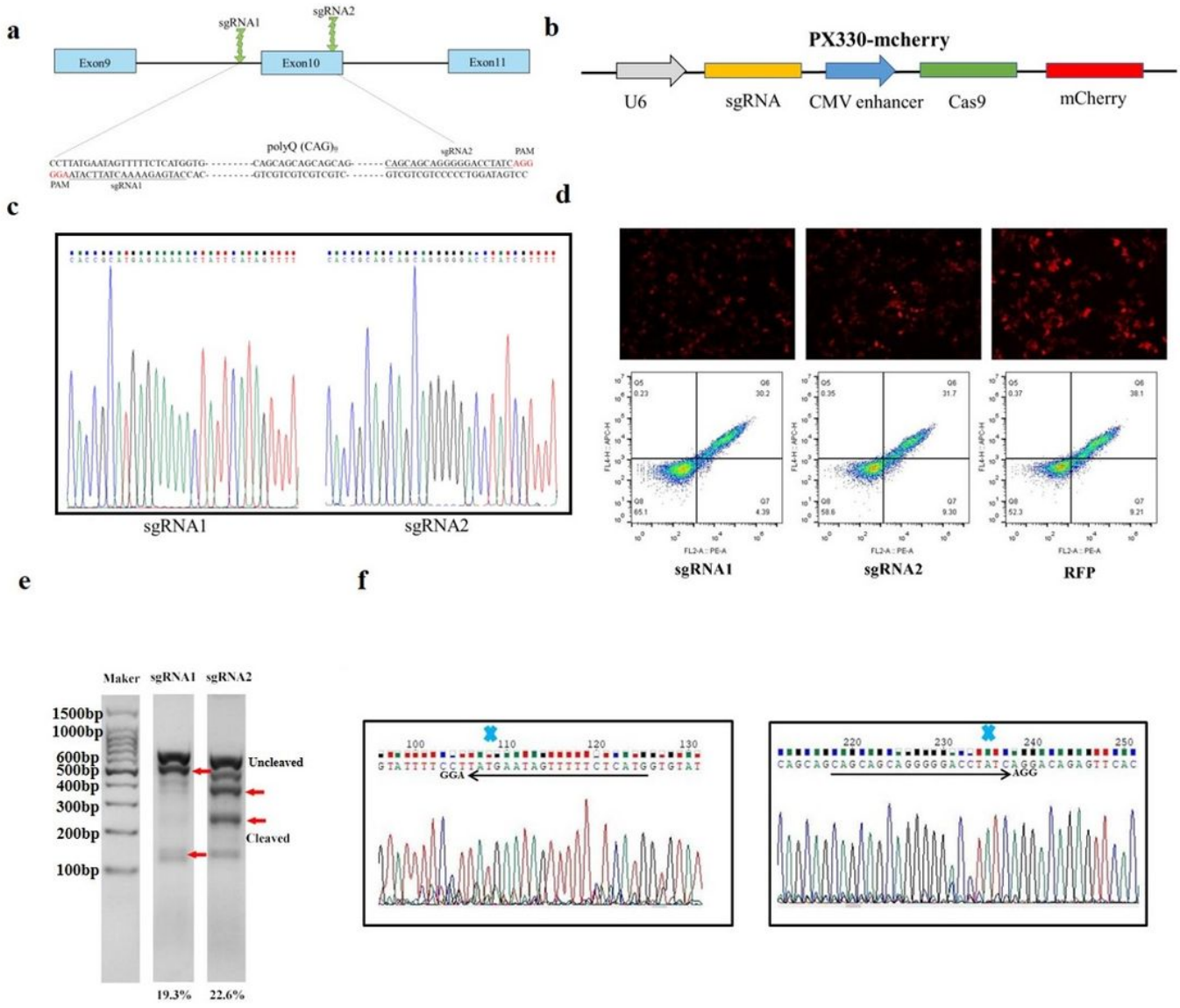


## Figure 1

Analysis of ATXN3-sgRNAs/Cas9n cleavage activity in HEK293T cells a. Targeted CAG repeats located in exon 10 of the ATXN3. SgRNA1 and sgRNA2 were designed to target the 5'- and 3'-repeat flanking sequences, respectively. Appropriate NGG PAM sequences are highlighted in red. b. Illustration depicting the CRISPR/Cas9 expression plasmid (PX330-mCherry) co-express Cas9 protein with the RFP reporter marker and sgRNA under the U6 promoter. c. Sequence of sgRNA1 and sgRNA2 successfully cloned into PX330-mcherry plasmid. d. The transfection efficiency of paired sgRNAs transfected into HEK293T cells were detected by immunofluorescence and flow cytometry, the transfection efficiency of cells was 30~50%. e. Analysis of ATXN3-sgRNA and wtCas9 activity in HEK293T cells by T7EN1 assay. The length of the targeting PCR product is 630 bp using primers pair (Uncleaved band). Cleaved bands were marked with red arrow, sgRNA1 and sgRNA2 cleavage efficiency reached 19.3% and 22.6%, respectively. f. After

gene editing with CRISPR/Cas9, the sequence trace after the break site comprised a mixture of signals derived from the unmodified and modified DNA.

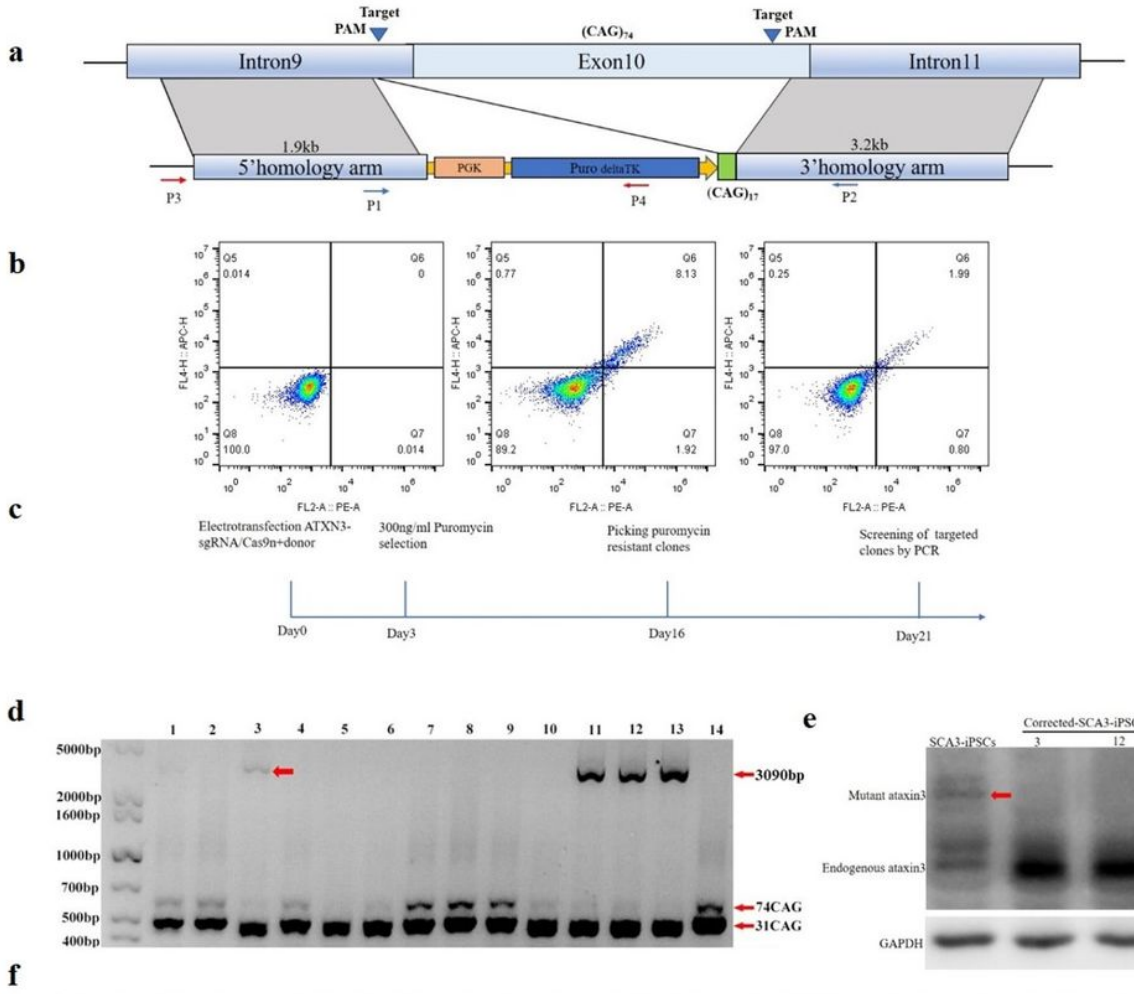


f

| Cells Transfected | Clones Screened (Puro) | CAG+ | Targeted |
|---|---|---|---|
| $5\times10^6$ | 116 | 14 (12.1%) | 2 (1.7%) |

## Figure 2

Correction of SCA3/MJD-iPSCs using Cre-loxP and CRISPR/Cas9 system a. Schematic depicting the donor DNA and Cre-loxP-based selection strategy used for targeting the ATXN3 locus, the targeting vector from pFlexible-DT with left and right arms of 1.9kb and 3.2kb respectively, and the correctly targeted allele with 17 CAG repeats and Puro cassettes inserted upstream of the corrected region. The targeted fragment sizes were verified by P1~P2 and P3~P4 primers. b. Quantification of the activity of ATXN3-targeted CRISPR-Cas9, detected by flow cytometry, negative cell population (the left figure), 10% RFP positive cells (the middle figure) and 2.8% paired sgRNAs/Cas9n positive cells (the right figure). c. Overview of the targeting workflow, including electroporation, selecting and screening. d. PCR-based

screening for successfully targeted iPSC clones, the positive clones (C3, C11, C12, C13) contained 510bp (31 CAG) and 3090bp using P1~P2 primers, while the mutant bands (639bp) indicated the 74 CAG repeats shown in red arrow. e. Verification of successful correction at the ATXN3 locus in selected iPSC clones by western blotting, the C3 and C12 clones indicated no expanded polyglutamine, the red arrow indicates the mutant ataxin3 protein. f. Summary of targeting efficiency by PCR screening, the targeted efficiency of CRISPR-Cas9 gene editing was 1.7%.

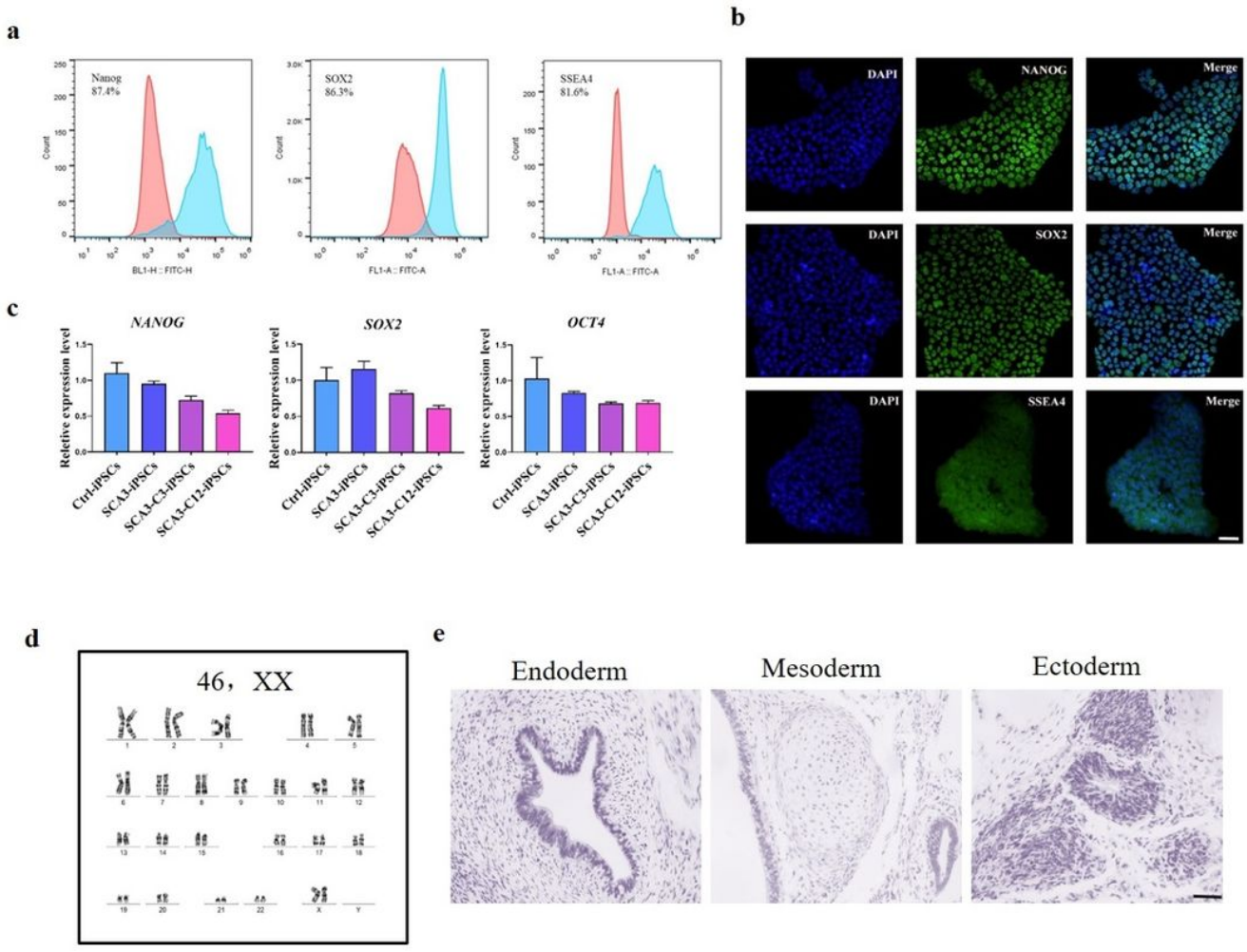


## Figure 3

Corrected SCA3/MJD-C3-iPSCs maintained pluripotent characteristics and normal karyotype a. Flow cytometry of pluripotent markers, including nuclear staining for NANOG, OCT4, and cell surface staining for SSEA4. b. Immunofluorescence staining of pluripotent markers, including nuclear staining for NANOG, SOX2 and cell surface staining for SSEA4. Scale bar: 100μm. c. Total RNA was isolated from iPSCs and analyzed with RT-qPCR. Primers used for NANOG, OCT4, and SOX2 specifically detect the transcripts from the endogenous genes. H1: embryonic stem cells (ESCs). Ctrl: Control healthy iPSCs. C-SCA3: Corrected SCA3/MJD-iPSCs. d. Karyotyping and G-band analysis showed corrected iPSC clones have a normal 46, XX karyotype. e. Teratomas comprised derivatives of the 3 germ layers. Scale bar: 100μm.

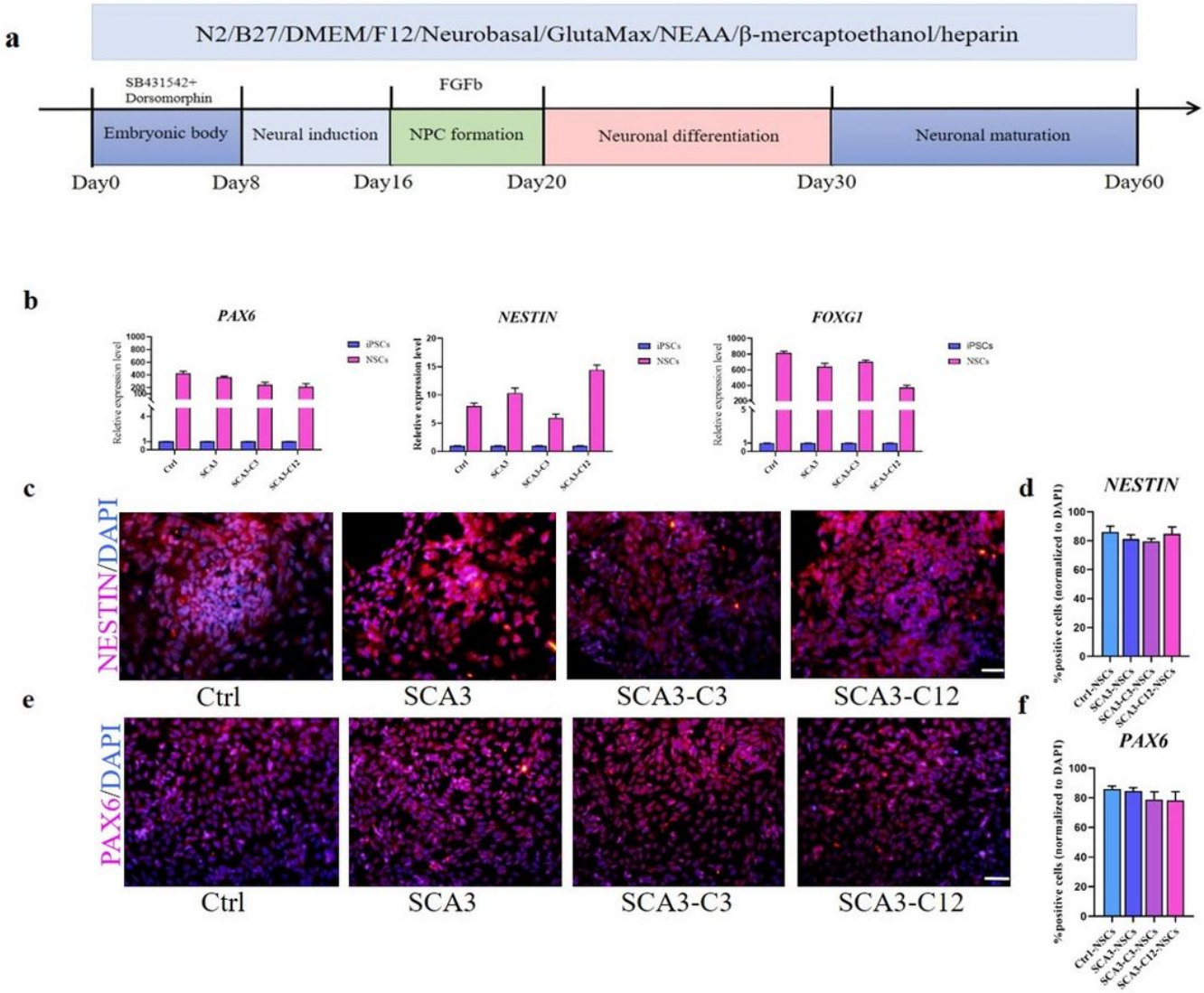


## Figure 4

The similar differentiation markers expressing in SCA3/MJD-NSCs and isogenic control SCA3/MJD-NSCs a. The scheme of neuronal differentiation protocol in vitro, the mature neurons were obtained about 60 days after differentiation. b-f. Neural induction resulted in robust expression of NSCs. b. NSCs markers, PAX6, NESTIN, FOXG1 (day 16) as measured by qRT-PCR (n=3 per sample independent biological replicates), the higher expression of NSCs markers in NSCs stage compared with iPSCs stage. c-f. PAX6 and NESTIN (day 16) as detected by immunocytochemistry. There was no difference in each group ($P>0.05$). Scale bar: 100μm. d, f All data were presented as mean±SEM. The data as determined by one-way ANOVA ($P=0.05$) and Bonferroni post hoc test among the groups. n=5 images for immunofluorescence.

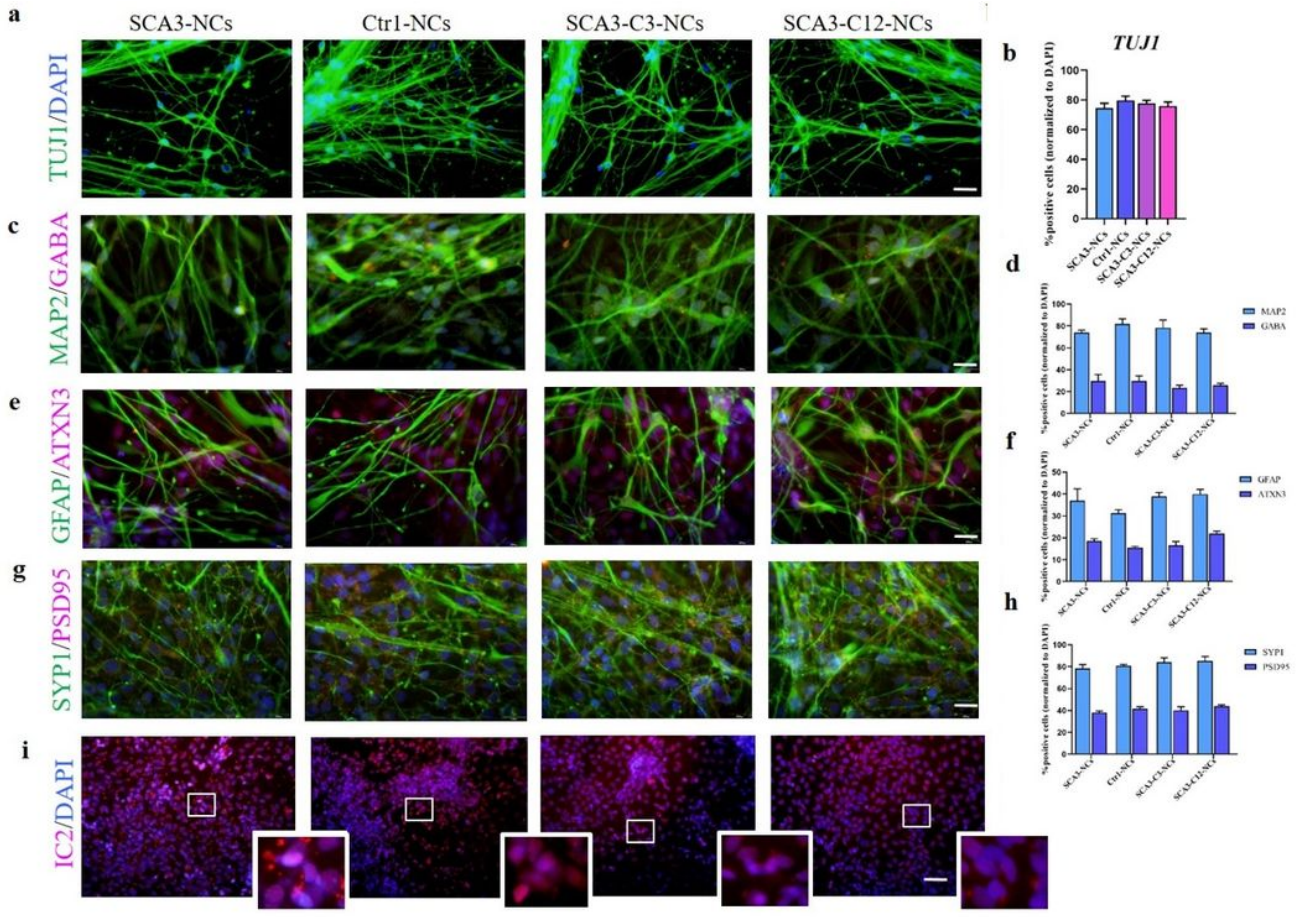


## Figure 5

Differentiation of SCA3/MJD and isogenic control SCA3/MJD-NSCs into forebrain cortical neurons a-f. Further differentiation resulted in neurons expressing β-III-tubulin, MAP2, GABA and GFAP, and the percentage of corresponding neuron markers were counted. Similar results were acquired with each cell lines in our study (P>0.05). Scale bar: 50μm. g-h. Representative images of iPSC-NCs stained with SYP1 and PSD95 on days 35~50, there was no difference about the expression of SYP1/PSD95 in each group (P>0.05). Scale bars 50μm. i. IC2 aggregates detected in SCA3/MJD-NCs compared with other group on days 50 (aggregates indicated in enlarged images). Scale bar: 100μm. b, d, f, h All data were presented as mean±SEM. The data as determined by one-way ANOVA (P=0.05) and Bonferroni post hoc test. n= (5, 6, 6, 6, 6, 6, 6) images for TUJ1, MAP2, GABA, GFAP, ATXN3, SYP1 and PSD95 neuronal markers expression.

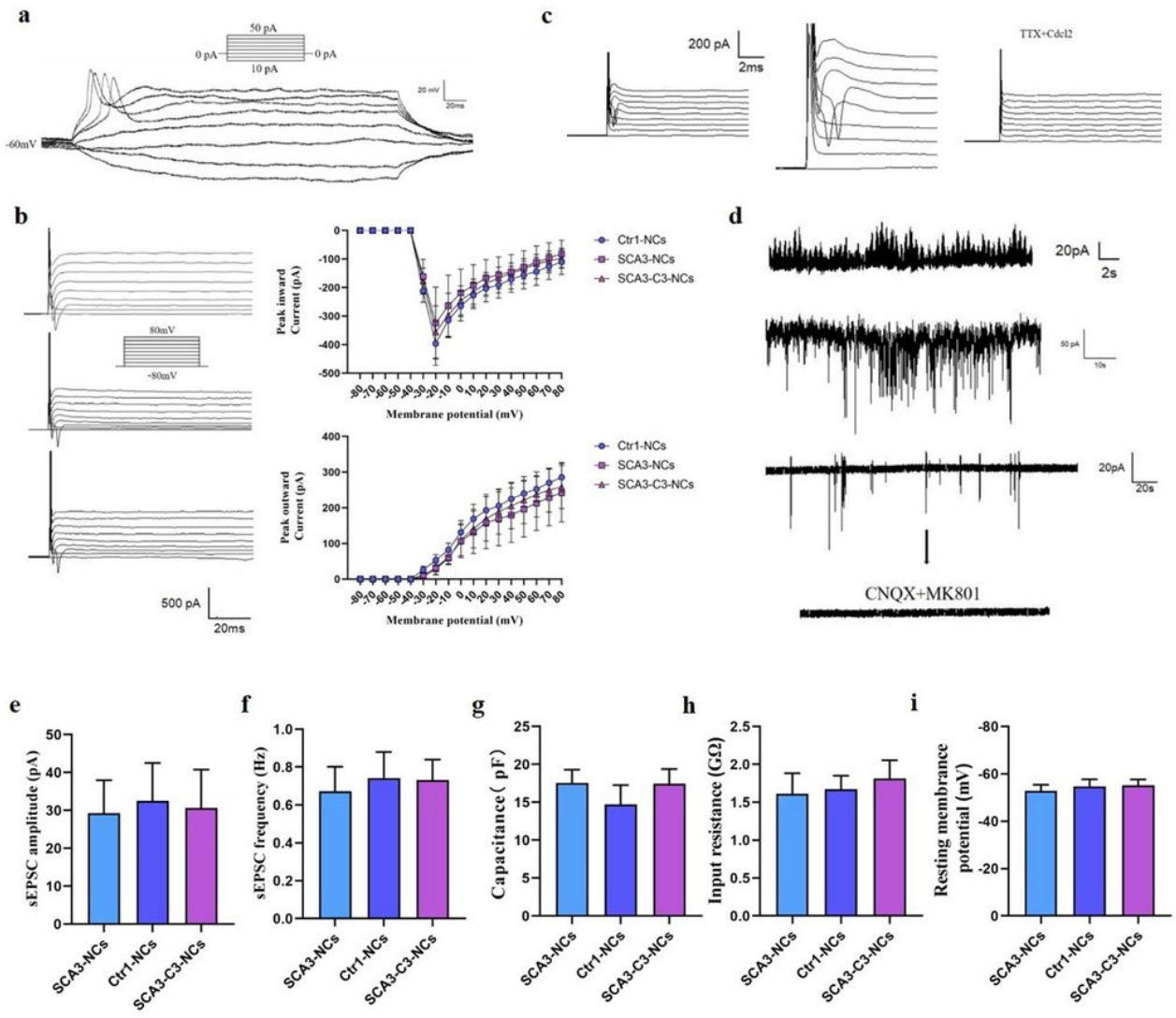


## Figure 6

Electrophysiological characterization of cortical neurons differentiated from SCA3/MJD and isogenic control SCA3/MJD-iPSCs a. Representative current clamp recording of evoked action potentials (APs) from SCA3-NCs after injection of step currents (10 to 50 pA). b. Voltage clamp recordings sustained inward and outward currents, in response to depolarizing voltage steps (-80 to 80 mV) in Ctrl, SCA3/MJD, and SCA3/MJD-C3 derived NCs, respectively. Quantification of inward and outward currents peak curves in Ctrl-NCs (n=10), SCA3/MJD-NCs (n=10) and SCA3/MJD-C3-NCs (n=10). Similar results were detected among the groups (P>0.05). c. The inward (Na+ and Ca+) and outward currents (K+) were blocked by TTX (1μM) and Cdcl2 (0.1mM) ion antagonist, respectively. d. Representative traces of inhibitory (upper image) and excitatory postsynaptic currents (bottom image), the excitatory postsynaptic currents were blocked by CNQX and MK801. e-f. The amplitude and frequency of sEPSC were similar in Ctrl, SCA3/MJD, and SCA3/MJD-C3 derived NCs (P>0.05). n=7 in three groups. g-i. The membrane capacitance, input resistance and resting membrane potential of Ctrl, SCA3/MJD, and SCA3/MJD-C3 derived NCs. No

significant difference was shown in three groups (P<0.05). n=7 in each group. All data were shown as mean±SED. The data as determined by one-way ANOVA (P=0.05) and Bonferroni post hoc test.

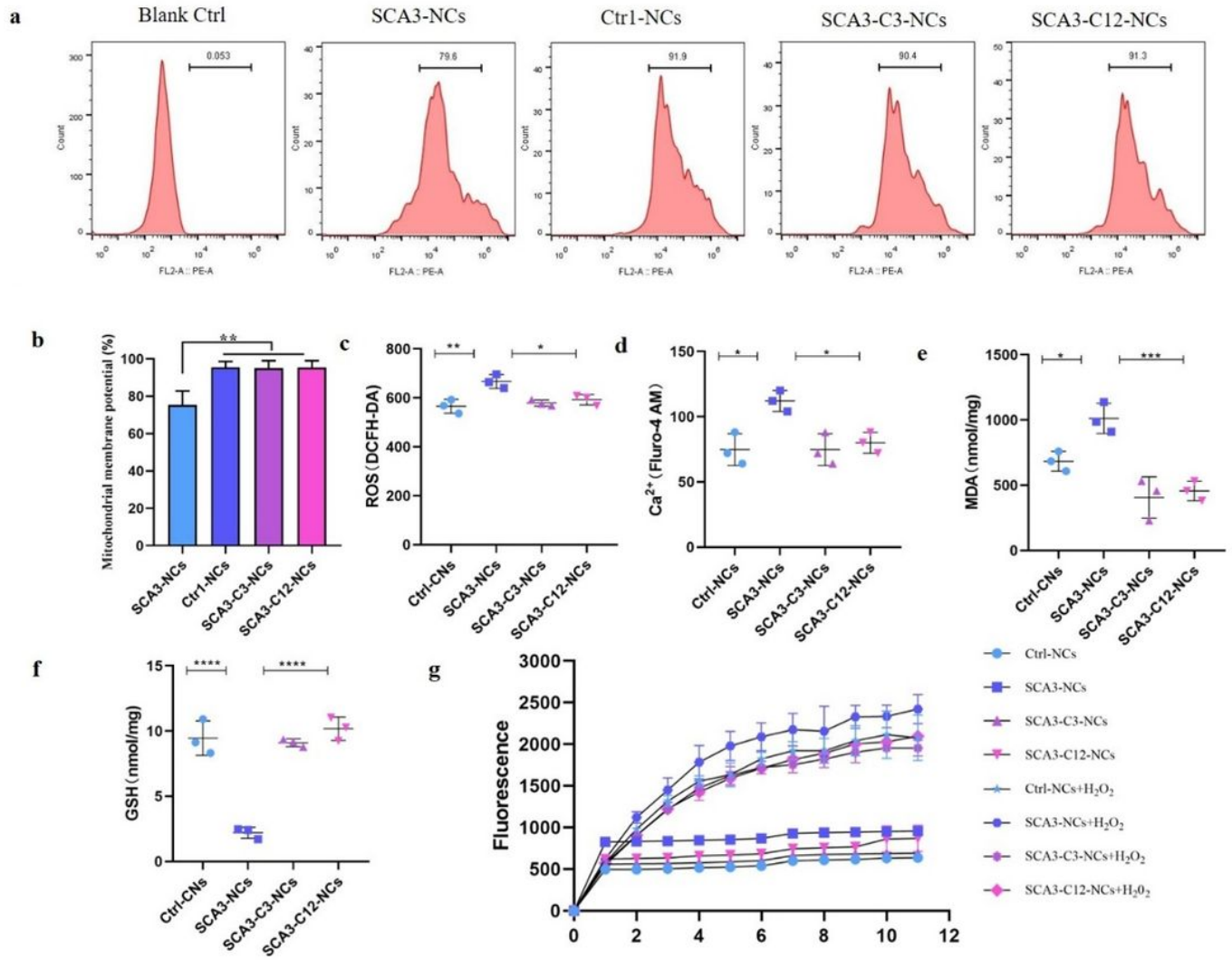


## Figure 7

The mitochondrial dysfunction and oxidative stress phenotypic characteristics rescued in isogenic control SCA3/MJD-NCs a-b. Mitochondrial membrane potential were decreased in SCA3/MJD-NCs compared with Ctrl-NCs, SCA3/MJD-C3-NCs and SCA3/MJD-C12-NCs (P<0.05). 3 independent biological replicates sample in four groups. c. Expression of ROS in each group. The ROS were increased in SCA3/MJD-NCs compared with other group, the corrected NCs rescued the ROS (P<0.05). d. Ca2+ concentration in Ctrl-NCs, SCA3/MJD-NCs, and isogenic control cell lines. The results indicated the intracellular Ca2+ was increased in SCA3/MJD-NCs, the corrected NCs rescued the Ca2+ concentration (P<0.05). e-f. MDA and GSH quantification across all four groups. The MDA levels were increased and GSH levels were reduced in SCA3/MJD-NCs compared with other groups, the corrected NCs rescued the MDA and GSH concentration (P<0.05). g. ROS levels and H2O2 induced ROS were recorded every 10min for a total of 10 times. The findings showed the ROS activated in SCA3/MJD-NCs, the corrected NCs

rescued the disease phenotypes (P<0.05). Data were showed as mean±SD (n=3). The data as calculated using one-way ANOVA (P=0.05), followed by Bonferroni post hoc test. *P<0.05 ,**P<0.01, ***P<0.005, ****P<0.001.

## Supplementary Files

This is a list of supplementary files associated with this preprint. Click to download.

- Supplementarymaterials.pdf